

NOTICE

**CERTAIN DATA
CONTAINED IN THIS
DOCUMENT MAY BE
DIFFICULT TO READ
IN MICROFICHE
PRODUCTS.**

LA-UR--93-1099

DE93 010737

TITLE
Momentum Induced by Laser-Tissue Interaction

AUTHOR(S)
Ronald S. Dingus, SD10/X-DO

SUBMITTED TO
International Society for Optical Engineering (SPIE)
Biomedical Optics '93
Laser Tissue Interaction IV Conference 1992
Los Angeles, CA
January 18-20, 1993

DISCLAIMER

This report was prepared as an account of work sponsored by an agency of the United States Government. Neither the United States Government nor any agency thereof, nor any of their employees, makes any warranty, express or implied, or assumes any legal liability or responsibility for the accuracy, completeness, or usefulness of any information, apparatus, product, or process disclosed, or represents that its use would not infringe privately owned rights. Reference herein to any specific commercial product, process, or service by trade name, trademark, manufacturer, or otherwise does not necessarily constitute or imply its endorsement, recommendation, or favoring by the United States Government or any agency thereof. The views and opinions of authors expressed herein do not necessarily state or reflect those of the United States Government or any agency thereof.

CONFIDENTIAL - For Official Use Only

Los Alamos National Laboratory, Los Alamos, New Mexico 87545

Available from National Technical Information Service, Springfield, Virginia 22161-4500

Los Alamos National Laboratory
Los Alamos, New Mexico 87545

CONFIDENTIAL
FOR OFFICIAL USE ONLY

MASTER
DISTRIBUTION OF THIS DOCUMENT IS UNLIMITED



ce

Momentum Induced by laser-tissue interaction

R. S. Dingus*

Los Alamos National Laboratory, Los Alamos, NM 87545

(* On leave to Strategic Defense Initiative Organization, Pentagon)

ABSTRACT

Impulsive momentum is imparted to residual tissue during pulsed-laser ablation because the mass ablated is generally ejected with a sizable velocity. Accurate measurements of the impulse are possible, which can provide an important monitor of the ablation process. Simple models can be used to predict the impulse under a variety of conditions; in some cases, complex radiation-hydrodynamic code calculations are required. In this paper, this modeling is discussed along with the dependence of momentum on the pulsed heating and target conditions. Momentum measurement techniques are discussed briefly. The behavior is explained in terms of dimensionless parameters and the impulse coupling coefficient as a function of incident fluence, which has a well defined threshold as well as a maximum. Complications in the mixed liquid-vapor phase are also addressed.

1. INTRODUCTION

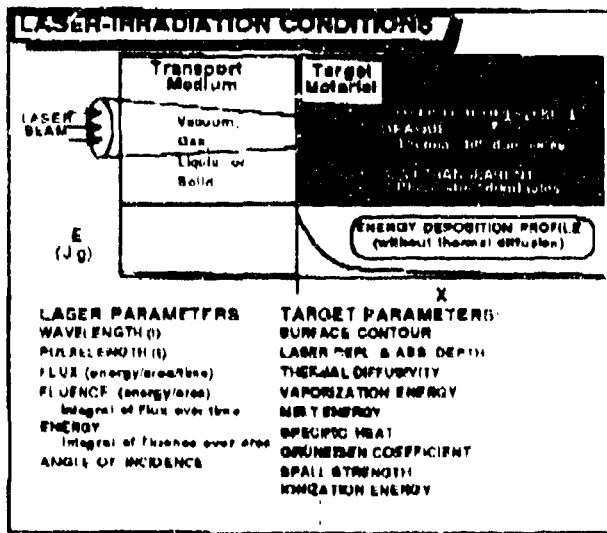


Figure 1. Illustration of many parameters, on which laser interaction depends.

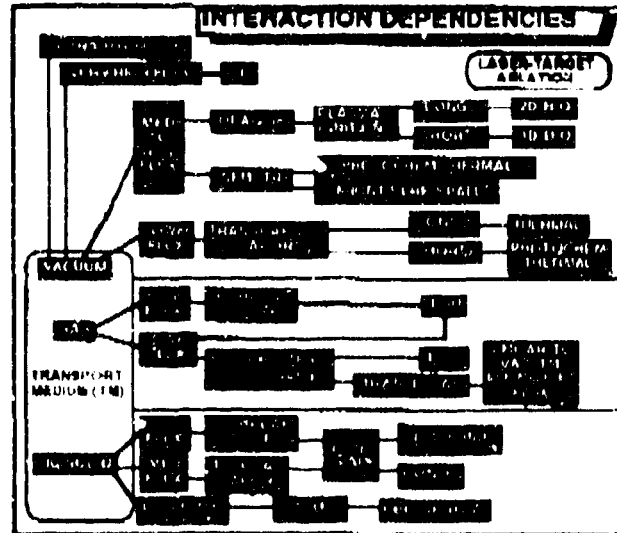


Figure 2. Categorization of processes associated with laser-target ablation.

Irradiation of tissue with a laser beam will result in significant tissue ablation (i.e., removal of tissue), if the intensity (i.e., energy flux, W/cm^2) is sufficiently large for a sufficiently long time. As illustrated in Figs. 1 and 2 and discussed in detail in Refs. 1 and 2, the physical processes resulting from intense laser irradiation of tissue depend strongly on many parameters associated with the laser beam, the (transparent) laser transport medium, and the laser-absorbing tissue. In any explanation of the process, it is important to first define which particular regime of behavior is involved; Fig. 2 offers a guide for categorizing the different regimes. The relative terms, such as low, medium and high fluxes, used in Fig. 2 are explained in Refs. 1 and 2 and depend on material and laser beam properties so that specific values for the boundaries of the regimes can only be defined after specification of many of the irradiation conditions.

All processes relating to the regimes identified in Fig. 2 involve ablation and therefore involve the generation of momentum, which is the subject of this paper. With potential clinical applications in mind, the emphasis in this paper is toward the regime in Fig. 2 for a gas transport medium at lower flux

for cases where the gas remains transparent to the laser. As indicated in Fig. 2, this regime is similar to that for a vacuum transport medium at low, medium or high flux; thus, for simplicity, this case will be discussed in depth. For the sake of discussion, it will be assumed that the ablation process is driven by thermal expansion or thermal decomposition; photochemical decomposition is another potential option but will not be discussed explicitly.

Although important to biomedical applications, little discussion in this paper will be given to the regime involving a liquid or solid transport medium. This regime involves much more complicated processes associated with contained vaporization³ where relatively long term restraint of material expansion impede application of the powerful conservation of momentum law.

2. BASIC MOMENTUM GENERATION PROCESS

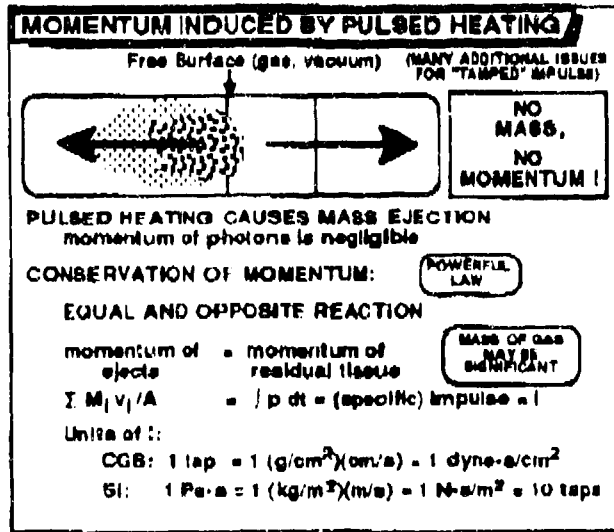


Figure 3. Momentum is imparted when pulsed heating causes mass ejection.

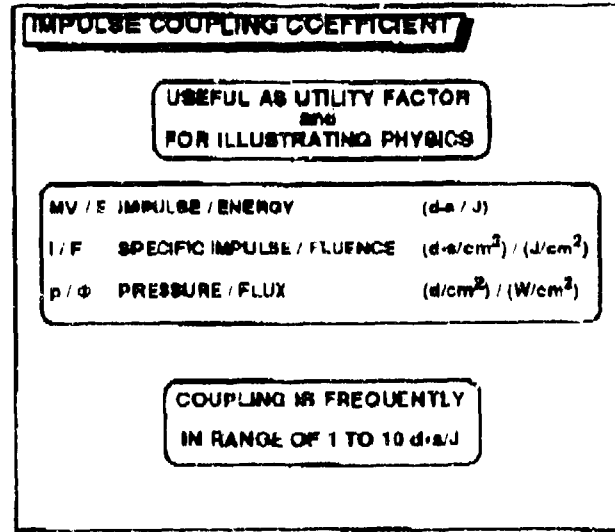


Figure 4. It is useful to define an impulse coupling coefficient, which is the ratio of momentum imparted to energy incident on the surface.

During the ablation of tissue by pulsed-laser heating (or photochemical decomposition), the mass ejected imparts a momentum to the tissue. The momentum imparted by the photons is negligible, so that for conditions in which no mass is ejected (i.e., no ablation), there is essentially no momentum imparted to the tissue. The powerful conservation of momentum law, which specifies that an action causes an equal and opposite reaction, indicates that, when the ejected mass completely separates from the remaining tissue, the momentum of the remaining tissue is equal to the momentum of the ejecta. The momentum, or impulse, of the ejecta is equal to the sum of the masses of the particles ejected times their respective velocities. Assuming uniform ablation over an area A, it is convenient to divide the momentum by A to give the specific impulse I. Then the integral of pressure over time applied to the tissue in the ablation region is equal to I. The CGS unit for I is referred to as a tap (1 tap = 1 (g/cm²)(cm/s) = 1 d-s/cm²). The SI unit is a Pa-s (1 Pa-s = 1 (kg/m²)(m/s) = 10 taps).

There are various other sources of pulsed heating besides lasers that can cause material ablation; some of these might have merit for biomedical applications. These potential pulsed sources include: electron beams, ion beams, microwaves, and x-rays. The merits of these alternative sources will not be considered in this paper, but much of the modeling discussion presented here is applicable to these beams.

3. IMPULSE COUPLING COEFFICIENT

It is convenient to define an impulse coupling coefficient as the momentum imparted per unit of irradiation energy incident on the target. Unfortunately, it is common to use the hybrid unit (mix of CGS and MKS units) of $d\cdot s/J$ for the coupling coefficient, although the SI unit of $N\cdot s/J$ is also used ($1 d\cdot s/J = 10^{-5} N\cdot s/J$). In reference to specific impulse per unit incident fluence, the coupling coefficient is obtained by dividing both the numerator and denominator by the area with units of $\text{tap}/(J/\text{cm}^2)$ or $\text{Pa}\cdot\text{s}/(J/\text{m}^2)$. Additionally, dividing (actually differentiating) the numerator and denominator by time gives a coupling coefficient in terms of pressure per unit incident flux with units of $(d/\text{cm}^2)/(W/\text{cm}^2)$ or $\text{Pa}/(W/\text{m}^2)$. The coupling coefficient is useful as a utility factor and also for illustrating the physics. For typical ablation conditions, as shown below, the coupling coefficient will frequently be within the range of 1 to 10 $d\cdot s/J$ for metal targets but it could be as high as 100 $d\cdot s/J$ for tissue (see Fig. 11).

4. TYPES OF ENERGY DRIVE

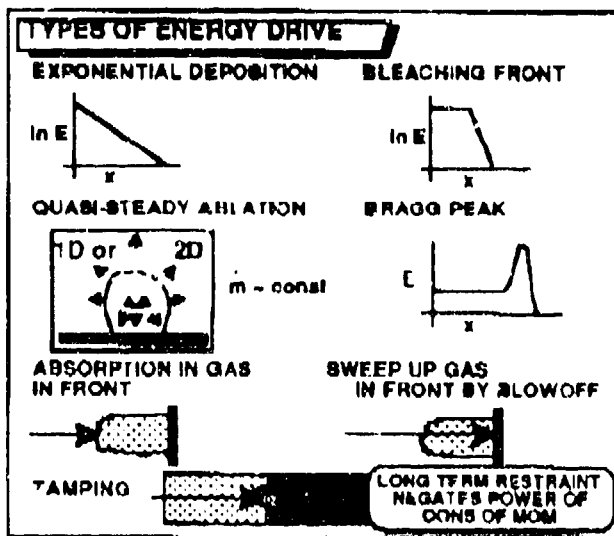


Figure 5. Types of energy drive.

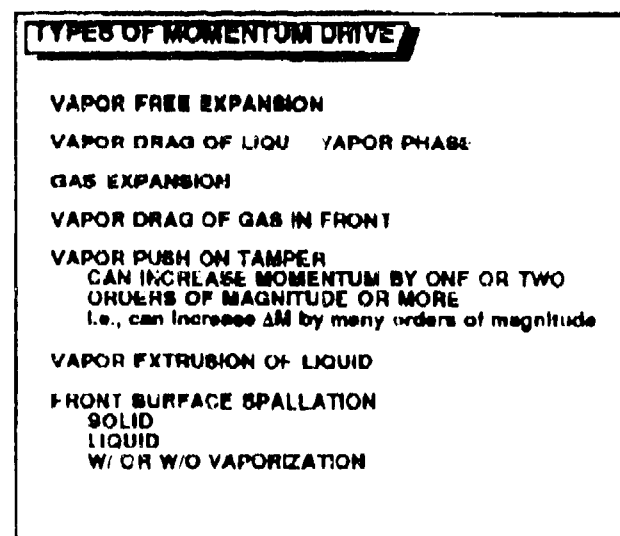


Figure 6. Types of momentum drive.

The momentum generation process is driven, first by energy, which provides the heat causing thermal expansion or thermal decomposition (vaporization)- either of which can cause mass to be ejected. Various types of heating processes are indicated in Fig. 5.

For semi-transparent tissue, the energy deposition decreases exponentially in the tissue; this case is discussed in detail in this paper.

Under certain conditions, such as when the energy density in the tissue reaches a certain level, the first part of the laser beam can cause the tissue to become transparent; this can produce a constant energy deposition into a depth, called the bleaching front, after which the energy density falls off exponentially.

Target material (in a vacuum) that is opaque will begin to vaporize at a time when the balance between absorbed laser flux and thermal diffusion flux raise the surface to the vaporization temperature. After vaporization begins, if the laser flux is sufficiently large, a plasma will be ignited. This plasma can be opaque to the laser beam and absorb essentially all of the rest of the laser pulse; ablation can be sustained by plasma radiation, leading to quasi-steady ablation during the rest of the pulse. When the laser pulse length is short compared to the time for blowoff material to traverse the diameter of the laser beam, relatively simple one dimensional (1D) modeling, as discussed below, can be used^{4,5}. For longer pulse lengths, the process is two dimensional (2D) and quantitative analysis requires complicated radiation hydrodynamic calculations^{6,7}, although simple modeling also provides some degree of

success for this case⁸.

The energy deposition for ion beams is quite different than for lasers; it is generally, nearly constant until near the end of the range, at which the deposition rises to the so called Bragg peak.

For a gas transport medium, if the laser flux is sufficiently large (but not too large so as to not be able to propagate to the target), a plasma will be ignited early in the pulse near an opaque target surface (or at imperfections or impurities on the surface of a transparent target), and the rest of the laser pulse will be absorbed at a front that propagates away from the target in the gas (called laser supported combustion, LSC, or laser supported detonation, LSD, waves)⁹.

At lower flux (and/or shorter wavelength, and/or lower gas pressure), a plasma will not be ignited but target ablation can still occur: the ablated target material will sweep up gas as it is ejected, which can substantially increase the momentum¹⁰.

Although the special features associated with each of the above processes must be carefully considered, simple modeling including these features is reasonably successful for each of them.

One more type is included in Fig. 5, namely, tamping, for which vapors generated by the pulsed heating are contained by surrounding liquid or solid. As indicated above and discussed in Ref. 3, this is a more complicated process, for which the modeling will not be discussed in this paper.

5. TYPES OF MOMENTUM DRIVE

Figure 6 lists various types of mass ejection processes, which basically drive the generation of the momentum after the heating.

Perhaps the simplest process is the free expansion into a vacuum of vapor created by laser deposition, in excess of the complete vaporization energy, for a short pulse incident on a semi-transparent material.

Some situations involve vapor expansion, where liquid droplets are mixed with the vapor or where the vapor is pushing against a liquid; this adds a major complication which is discussed further below.

Expansion of a heated region of gas into surrounding colder gas occurs for LSC and LSD waves⁹.

Target ablation vapors (and droplets) expanding into a transport medium that consists of a transparent gas involve the drag of the gas by the ablated material¹⁰.

Vapors created behind a tamper, which breaks free, can result in a momentum one or two orders of magnitude larger than for the untamped case because of the large increase in ejected mass³.

For ablation involving vaporization from a liquid pool (either the target might have been a liquid initially or it might have been a solid and the liquid was formed by energy deposition from the laser or from thermal diffusion), the vapor back pressure can cause liquid ejection by extrusion. This extruded mass can be ejected with a very small relative velocity and can be ejected at a grazing angle to the surface; if so, it will impart little momentum to the surface. This can be a serious complication when trying to associate measurements of target mass loss with the ablation mass to be used in momentum calculations¹¹.

For sufficiently short heating pulselengths, liquid or solid target material can be ablated by front surface spallation^{12,13,14}; the threshold for this spallation process is at temperatures below the vaporization threshold, but even with vaporization, the process can enhance the removal of material behind the vaporized region.

6. SIMPLE MODELING

The impulse induced by laser deposition can be predicted with reasonable accuracy using simple modeling based upon the energy density in the blowoff as illustrated in Fig. 7. In the discussion of this model, the heating is assumed to be at a surface where the ablated tissue can escape freely. For simplicity, the presence of gas in front of the irradiated tissue surface will be ignored; however, in some cases, the mass of the gas swept up by the ablated target material can be large compared to the ablated mass, in which case, the impulse will be significantly larger than predicted by the model presented here.

Suppose that for a laser fluence F_0 incident on the tissue, a total mass M_0 is ejected with a kinetic energy K from a region of the tissue having area A . Then $k = K/A$ and $m_0 = M_0/A$ are the kinetic energy per unit area and mass per unit area of the ejected material. An upper limit for the momentum per unit area (call it I_{0U} for impulse upper limit) imparted to the tissue can be calculated by assuming

"final state" internal energy density, that is, the internal energy density that existed at the time that the mass stopped communicating back with the residual target; E_0 is not necessarily the same for all of the mass ejected, but in the modeling in this paper, E_0 is assumed to be constant.

It is significant to note that the impulse I is proportional to $(m_0 k)^{1/2}$ and that an upper limit is known for k , namely F_0 . The mass m_0 is generally much harder to estimate than k ; so that the major uncertainty in predicting I is generally in knowing the mass ejected rather than in knowing the kinetic energy in the mass ejected. Also, the impulse is insensitive to the distribution of the kinetic energy within the mass ejected; for example, if 99% of the kinetic energy is contained by only 1% of the mass ejected, then the momentum is still 20% of the upper limit value (the upper limit corresponds to 99% of the kinetic energy being contained within 99% of the mass ejected, i.e., uniform energy density).

7. EXPONENTIAL ENERGY DEPOSITION

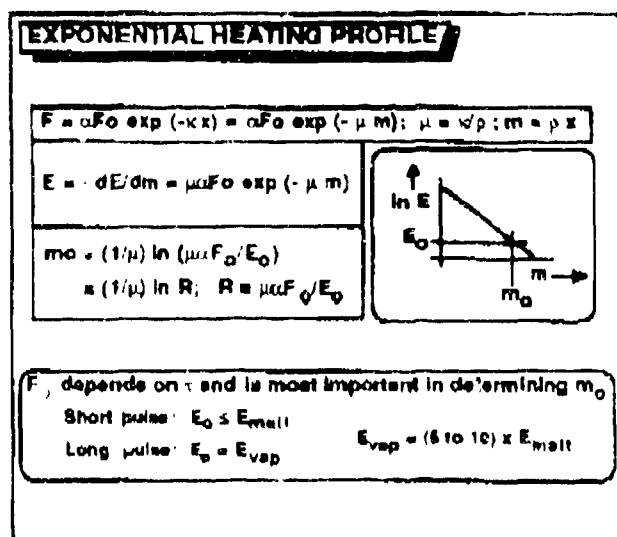


Figure 8. Exponential energy density profile.

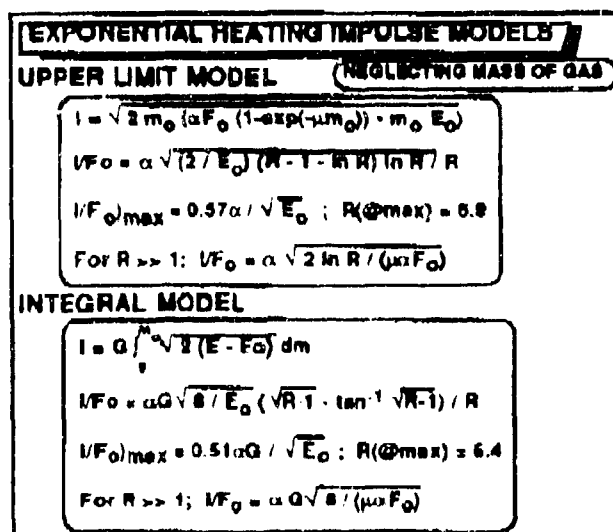


Figure 9. Upper limit and integral impulse models for exponential heating.

Figure 8 gives equations needed in the model for exponential energy deposition. Figure 9 gives analytic solutions for the impulse for exponential energy deposition, respectively using the upper limit model (Eq. 1) and the integral model (Eq. 2). Let κ be the linear absorption coefficient for the laser beam, x be the distance into the tissue from the front surface, ρ be the density of the tissue, $\mu = \kappa/\rho$ be the mass absorption coefficient, $m = \rho x$ be the mass distance into the material. Then the fluence F at depth x (or m) in the tissue is $F = \alpha F_0 \exp(-\kappa x) = \alpha F_0 \exp(-\mu m)$ and the absorbed energy density E absorbed at depth x (or m) in the tissue is

$$E = -dF/dm = \mu \alpha F_0 \exp(-\mu m). \quad (3)$$

If we assume that all mass is ejected that has an energy density E greater than E_0 , then $F_0 = \mu \alpha F_0 \exp(-\mu m_0)$ or

$$m_0 = (1/\mu) \ln(\mu \alpha F_0 / E_0) = (1/\mu) \ln R \quad \text{where } R = \mu \alpha F_0 / E_0. \quad (4)$$

Note that $\mu \alpha F_0$ is the deposited energy density at the front surface of the tissue, so that R is the ratio of the front surface dose to the critical energy density; or, noting that E_0/μ is the blowoff-threshold fluence, R is the ratio of the fluence transmitted through the front surface to the blowoff threshold

fluence. Putting Eqs. 3 and 4 into Eq. 2, integrating and dividing through by F_0 to give the impulse coupling coefficient gives

$$I/F_0 = \alpha G (8/E_0)^{1/2} (R-1)^{1/2} - \tan^{-1}(R-1)^{1/2} / R \quad \text{Integral Model} \quad (5)$$

It can be shown that the maximum of Eq. 5 occurs for $R = 6.4$ and that the value of Eq. 5 at $R = 6.4$ is

$$(I/F_0)_{\max} = 0.51 \alpha G / (E_0)^{1/2} \quad \text{Integral Model} \quad (6)$$

Following this same approach for the upper limit model, $\beta = \alpha F_0 \exp(-\mu m_0)$ is the fluence at depth m_0 ; using this and Eq. 4 with Eq. 1 gives

$$I/F_0 = \alpha (2/E_0) (R - 1 - \ln R) \ln R)^{1/2} / R \quad \text{Upper Limit Model} \quad (7)$$

It can be shown that the maximum of Eq. 7 occurs for $R = 6.9$ and that the value of Eq. 7 at $R = 6.9$ is

$$(I/F_0)_{\max} = 0.57 \alpha / (E_0)^{1/2} \quad \text{Upper Limit Model} \quad (8)$$

Comparing Eqs. 6 and 8 shows that $(I/F_0)_{\max}$ differs by only about 10% between the integral model and the upper limit model. Also, the maximum occurs at about the same value of R .

For long pulselengths, the only mechanism (neglecting photochemical decomposition) for mass ejection is vaporization by thermal decomposition. In this case, the critical energy E_0 is equal to the (complete) vaporization energy. For sufficiently short pulselengths, ablation can occur by front surface spallation at a much lower threshold energy^{12,13}; for solid targets, the critical energy E_0 is sometimes near the melt energy because the spall strength decreases to near zero at melt. Thus, the threshold is much lower for short pulselengths because the vaporization energy is typically about 5 to 10 times larger than the melt energy. At intermediate pulse lengths, the process is more complicated as discussed below.

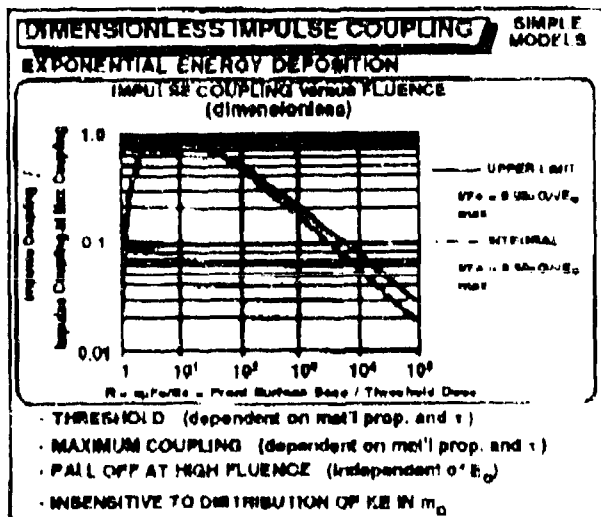


Figure 10. Dimensionless impulse coupling. Impulse coupling coefficient divided by maximum coupling versus fluence divided by blowoff-threshold fluence.

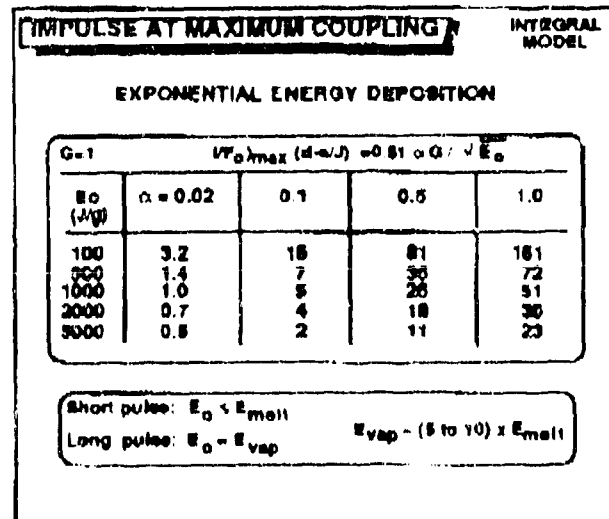


Figure 11. Impulse at maximum coupling versus absorptivity and critical energy density.

In Fig. 10, Eq. 5 divided by Eq. 6 is plotted versus R and Eq. 7 divided by Eq. 8 is plotted versus R . Figure 10 shows that the shape of the dimensionless curves are similar for integral and upper limit models, which (combined with the 10% difference in $1/F_{0max}$) illustrates the insensitivity of impulse to energy distribution in the blowoff mass. Figure 10 also illustrates the impulse threshold, which depends on material properties and pulselength, the maximum in the coupling coefficient and the fall off in coupling at high fluence, where the impulse becomes independent of the critical energy density. Figure 11 gives values for the maximum coupling for the integral model from Eq. 6 for various values of α and E_0 . As shown in Fig. 11, the maximum coupling generally ranges from about 1 to 100 d-s/J, depending on the target material and the laser pulselength and wavelength. Perhaps it should be emphasized that although the impulse coupling (which is the efficiency with which deposited energy generates momentum) referred to in Figs. 10 and 11 has a maximum value at some fluence, the impulse always increases as the fluences increases, when above the threshold.

8. MIXED PHASE COMPLICATION

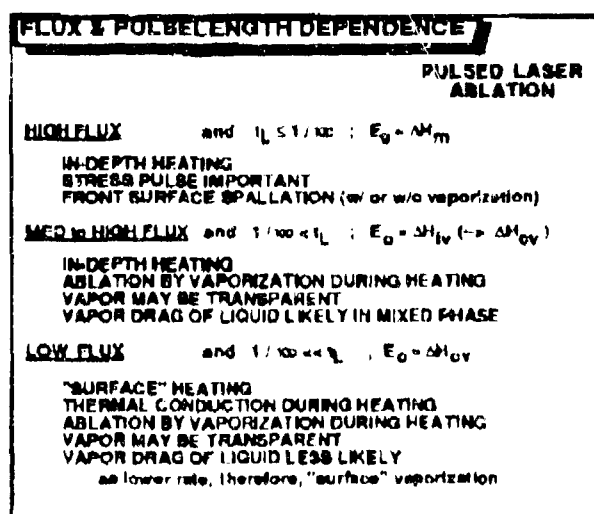


Figure 12. Flux and pulselength dependence.

Figure 12 shows the dependences of the process and the critical energy on flux and pulselength.

When the laser pulselength, t_L , is short compared to $1/(\kappa)$, the time for a sound wave to traverse one laser absorption depth ($1/\kappa$), then thermal expansion can not occur during the heating, front surface spallation becomes possible, and E_0 becomes approximately the melt energy ΔH_m or smaller^{12,13}.

When the laser pulselength is long compared to $1/(\kappa)$ and the laser flux is sufficiently small, but large enough to cause vaporization, then vaporization will begin during the laser pulse and likely at the front surface where the temperature generally will be the largest (suppose that the vapors are transparent to the laser beam). The cooling associated with vaporization will clamp the surface at the vaporization temperature. If the laser flux is small enough, energy transport by thermal diffusion will prevent any significant temperature rise in depth above the front surface temperature. Also, due to the slow process, any vaporization at nucleation sites in the liquified layer (most materials don't sublime under these conditions) should be able to migrate to the surface as the bubbles grow rather than explosively erupting. In this case, E_0 should be equal to the complete vaporization energy, ΔH_{OV} .

However, at larger laser fluxes, for materials with a significant absorption depth, the material behind the surface can become super heated, which can lead to explosive eruptions, referred to as the "popcorn" effect. If the flux is sufficiently large, as discussed further below, partial vaporization in the mixed phase region will simply drag much of the melted material during expansion of the vapors; then E_0 would be expected to be approximately equal to the incipient vaporization energy, ΔH_V .

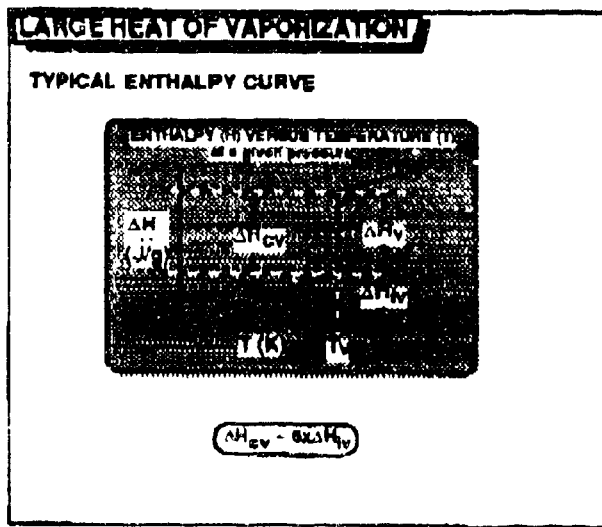


Figure 13. Large heat of vaporization.

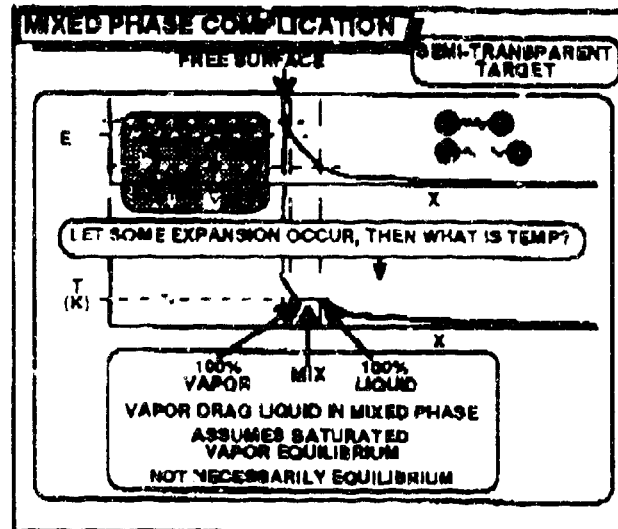


Figure 14. Mixed phase complication.

The typical enthalpy curve in Fig. 13 conceptually illustrates why this mixed phase complication is so significant. The enthalpy plot gives the amount of energy (per unit mass) required to change the temperature at a given pressure. This figure is based on constant specific heat and shows the step in enthalpy at the liquid-vapor phase change (assuming a liquid for the initial condition; there is also a step for the solid-liquid phase change but the step is generally much smaller). The incipient vaporization energy, ΔH_{iv} , is the energy required to heat the material from ambient temperature to the vaporization temperature, T_v , but to leave it in the condensed phase (most materials are liquids at this temperature at low pressures). The heat of vaporization, ΔH_v , is the energy required to take it from the condensed phase (liquid) to the vapor phase (i.e., to break the molecular or atomic bonds), while holding the temperature constant. The complete vaporization energy is the sum, $\Delta H_{iv} + \Delta H_v$. An important point is that the complete vaporization energy is typically about 5 times the incipient vaporization energy ΔH_v . Also, if the material remains in thermodynamic equilibrium, then as energy is added (at constant pressure) between ΔH_{iv} and ΔH_{cv} , more and more material is vaporized (the vapor fraction is $(\Delta H - \Delta H_{iv})/(\Delta H_v)$) but the temperature remains at the vaporization temperature, T_v , until all the material is vaporized at ΔH_{cv} .

Figure 14 addresses the complications originating from mixed phase blowoff, which occur at relatively long pulselengths and sufficiently large fluxes. In the top part of Fig. 14, laser deposited energy density is plotted versus depth in the material, with the enthalpy curve superimposed in front. Below that, the temperature is plotted versus depth, assuming that enough expansion has occurred slowly to let the pressure relax. This illustrates that, assuming thermodynamic equilibrium, all of the material with E between ΔH_{iv} and ΔH_{cv} will be at temperature T_v , but the front portion of this region will be completely vapor and the back portion will be completely liquid. If the laser energy was deposited in a short time compared to that for significant vapor expansion to occur (but possibly long compared to $1/\kappa c$), then as the material vaporizes and expands in this mixed phase region, the vapor will likely drag off most of the liquid in this region; but just exactly how much liquid is drug off and how much momentum it carries is difficult to estimate. Also, the assumption of thermodynamic equilibrium will at least sometimes be invalid. For longer pulse lengths, as described above, vaporization at the eroding surface can, in some cases, keep up with the laser flux, but superheating can occur in depth, followed by eventual nucleation and explosive eruption.

9. 1D PLASMA ENERGY BALANCE MODEL

A model⁵ that is rather different from the exponential energy deposition models, but based upon essentially the same principals, is illustrated in Fig. 15. This 1D Plasma Energy Balance (PEB) model is for an opaque target in a vacuum. Early in the pulse, the target begins to vaporize and a plasma is ignited that becomes nearly opaque to the laser. This plasma radiates energy in all directions, some of which reaches the target to sustain ablation. As indicated in Fig. 15, the model, which allows plasma expansion in only one dimension (1D), is based upon an overall energy balance and also an energy balance at the ablation surface. Then by assuming a constant ablation rate throughout the pulse and constant temperature for the plasma, all physical variables for the process can be solved for, including: the ablation mass and velocity and thus momentum; the plasma density, temperature and pressure; the radiation from the plasma; and the attenuation of the laser beam and of the radiation from the plasma. Generally, the reflectivity of the target is not known under the conditions of interest for this model. In comparing predictions from this model with impulse data (see below), the reflectivity has been taken as a free parameter to fit the data; there are no other free parameters in the model.

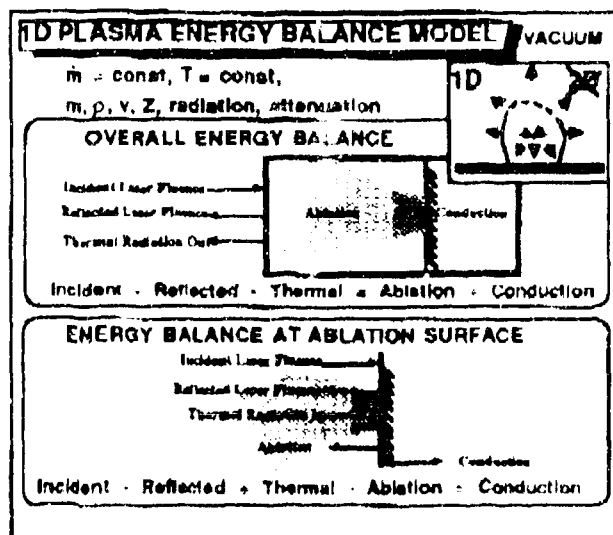


Figure 15. One dimensional plasma energy balance model.

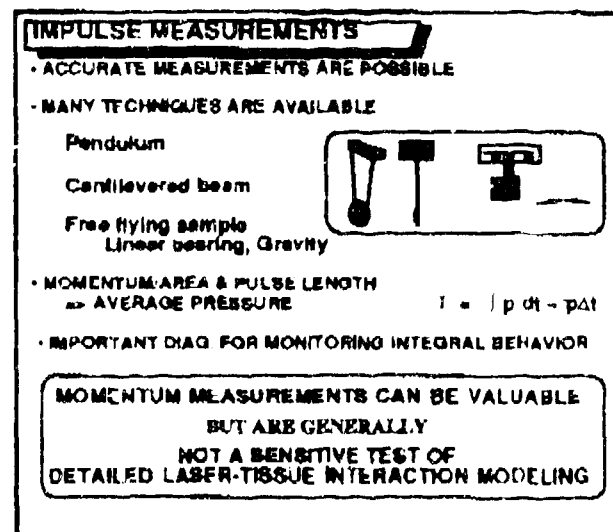


Figure 16. Impulse measurements.

10. IMPULSE MEASUREMENTS

Figure 16 illustrates various impulse diagnostic techniques with which accurate measurements are possible. The duration of the pressure pulse associated with laser ablation is generally about one to two times the laser pulse length, so that combining the momentum measurement with the ablation area and the pulse length allows an estimate of the average pressure applied during the ablation. Conversely, pressure diagnostics can also be used to measure the pressure and the area under the pressure versus time curve can be integrated to deduce the momentum; generally, this is not nearly as accurate as measurement with a momentum gauge. Because momentum closely correlates with the mass ablated, momentum measurements can be a valuable diagnostic for biological research as well as for a monitor for clinical applications. Also, as the impulse increases, the potential for damaging side effects to tissue increases, so that it might be important to limit impulse to tolerable levels during clinical applications. Because the momentum is an integral of the entire ablation process, it is generally not a sensitive test of detailed laser-tissue interaction modeling.

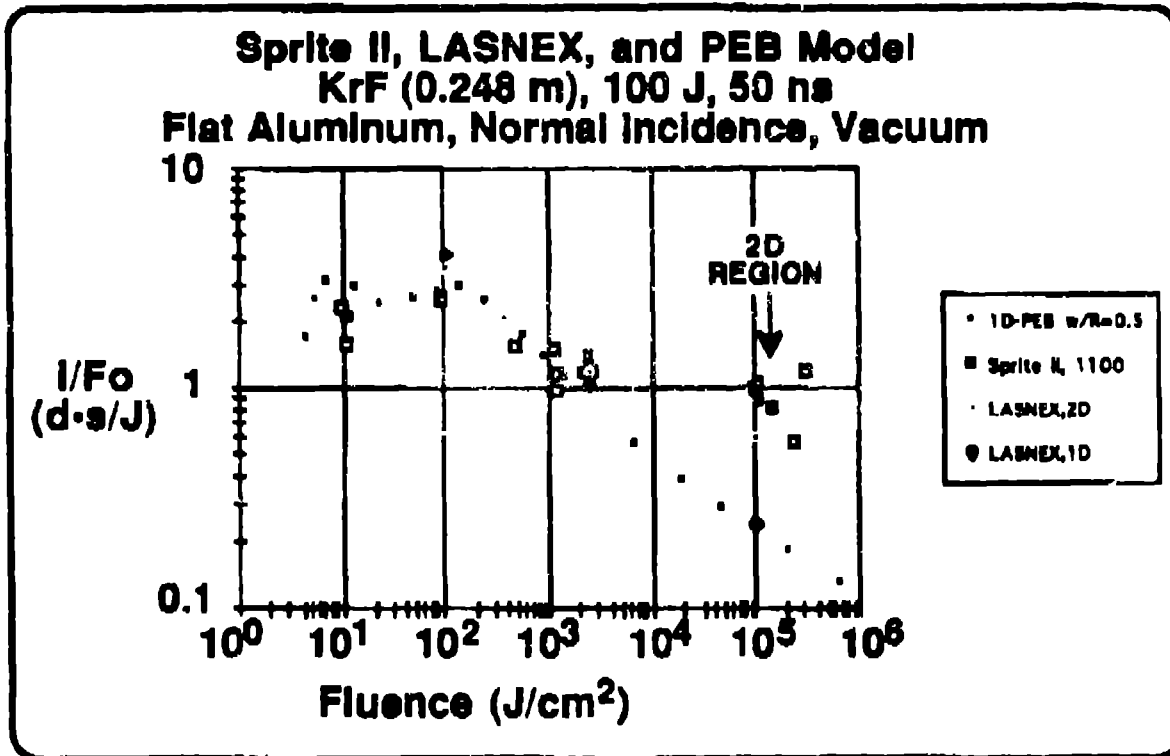


Figure 17. Sprite II impulse data compared with calculations.

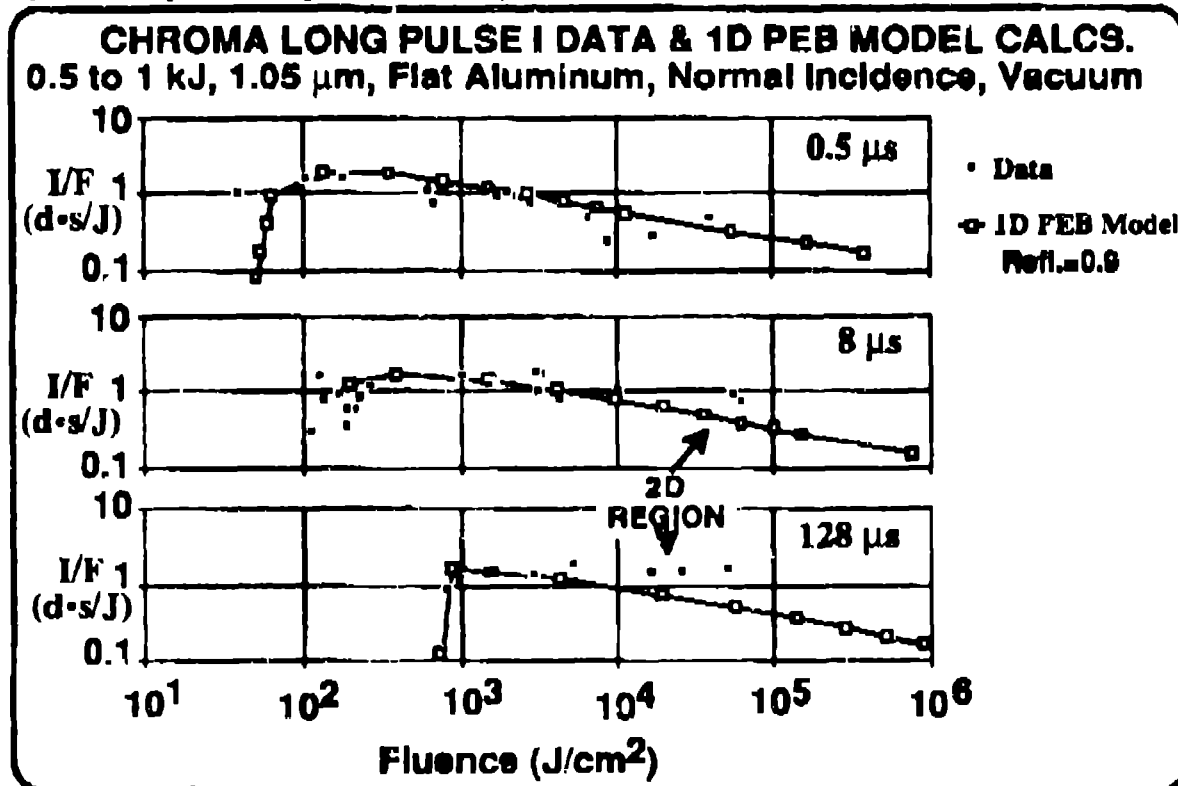


Figure 18. Chroma data compared with calculations.

11. COMPARISON OF IMPULSE DATA WITH CALCULATIONS

Figure 17 gives data taken during Series II of experiments at the Sprite laser at the Rutherford-Appleton Laboratory¹⁰. The 1D PEB model predictions agree well with the data, when a reflectivity of 0.5 is used, except at fluences above about 10^4 J/cm². At these high fluences, the blowoff becomes two dimensional (2D) and the 1D PEB model breaks down. Figure 17 includes LASNEX both 1D and 2D radiation-hydrodynamic code calculations at a fluence of 10^5 J/cm²; the 1D LASNEX calculations agree with the 1D PEB predictions⁵ and the 2D LASNEX calculations^{6,7} agree reasonably well with the data.

Figure 18 gives data taken during Long-Pulse Series I experiments at the Chroma laser at KMS Fusion in Ann Arbor, Michigan¹¹. The trend is similar as for Sprite except that a reflectivity of 0.9 was required to fit the data; the reflectivity principally affects the fluence at which the impulse threshold occurs. Again, as expected, the 1D PEB model does not fit the data in the 2D regime.

12. SUMMARY

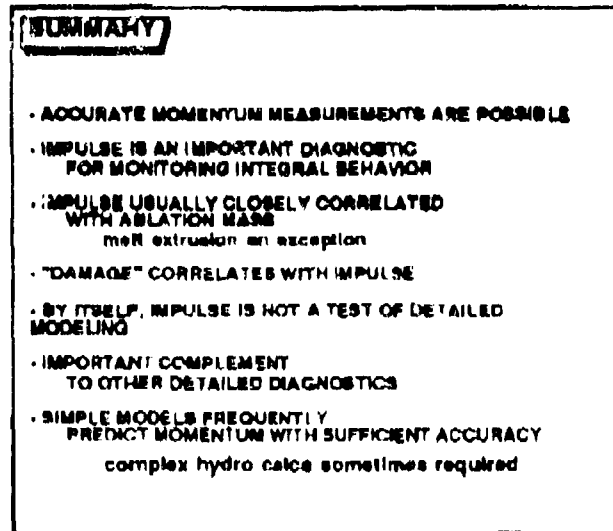


Figure 19. Summary.

Summarizing (see Fig. 19), accurate momentum measurements are possible and should have value for both research and clinical applications. Impulse is an important diagnostic that could be used to monitor integral behavior in clinical applications. Impulse is usually closely correlated with ablation mass except for mass extruded from the target by vapor back pressure, which may be ejected at very low velocity and at grazing angles. Damaging side effects should increase with impulse so limiting impulse to tolerable levels may be advantageous. Impulse is a measure of the integrated ablation process and is not a sensitive test of detailed modeling. However, it can be an important complement to other detailed diagnostics. Simple models are frequently adequate to predict impulse with sufficient accuracy but in some regimes complex radiation hydrodynamic code calculations are required.

8. REFERENCES

1. R. S. Dingus et al, *Pulsed laser effects phenomenology, Thermal and Optical Interactions with Biological and Related Composite Materials*, Michael J. Berry, George M. Harpole, Editors, Proc. SPIE 1064, pp. 66-76 (1989).
2. R. S. Dingus, *Laser Ablation Processes, Lasers, Sensors, and Spectroscopy Solid State Lasers III*, Proc. SPIE 1627 (1992).
3. R. S. Dingus, *Laser-induced contained vaporization in tissue*, in *Laser-Tissue Interaction III*, Steven L. Jacques, Editor, Proc. SPIE Vol. 1646, pp. 266-274(1992).
4. R. S. Dingus, *Phenomenology of Optical-Laser-Induced Impulse in Vacuo*, Los Alamos National Laboratory internal document SDR/U:84-92 (March 8, 1984), to become document LA-10113.
5. R. S. Dingus and S. R. Goldman, *Plasma Energy Balance Model for Optical laser-induced Impulse in Vacuo*, Proceedings of the International Conference on Lasers '86, pp. 111-122, Orlando, Florida (1986).
6. S. R. Goldman et. al, *Laser Matter Interaction at Intensities of 10^{12} W/cm² and Below*, SPIE Volume 1279 Laser-Assisted Processing 11, 1-8 (1990).
7. S. R. Goldman et al, *Modelling of Laser Matter Interaction at Intensities below 10^9 W/cm²*, Plasma Physics Divisional Meeting of the American Physical Society, 1990.
8. N. G. Basov, V. A. Gribkov, O. N. Krokhni, and G. V. Sklizkov, *High Temperature Effects of Intense Laser Emission Focused on a Solid Target*, Soviet Physics JETP, vol. 27, No. 4, pp.575-582, (1968).
9. A. N. Perri, *Theory for momentum transfer to a surface with a high-power laser*, Physics of Fluids, Vol. 16, no. 9, pp. 1435-1440, 1973.
10. R. S. Dingus, R. Green, T. R. King, W. Z. Osborne, and C. R. Phipps, Jr., *Single Pulse Laser Effects Measurements at 248 nm using Sprite*, pp 145-166 in Proceedings of the SUBWOG 6P Joint US/UK Workshop AVIS156, Single Pulse Laser Effects Report Session, compiled by R. S. Dingus, Los Alamos National Laboratory Report LA-UR-87-313, January 1987.
11. R. G. Watt, et al., *The Long Pulse Phase I Experiment*, Defense Nuclear Agency Report DNA-Tr-87-118 (1987).
12. R. S. Dingus and R. J. Scammon, *Grüneisen stress induced ablation of biological tissue*, Laser Tissue Interaction II, Steven L. Jacques, Editor, Proc. SPIE 1427, pp. 45-54 (1991).
13. R. S. Dingus and R. J. Scammon, *Ablation of Material by Front Surface Spallation*, J. C. Miller and R. F. Haglund, Jr. editors, Lecture Notes in Physics-389, Laser Ablation Mechanisms and Applications, Springer-Verlag, New York, 1991.
14. G. Paultauf, *Study of different ablation models by use of high-speed-sampling photography*, in *Laser Tissue Interaction III*, Steven L. Jacques, Editor, Proc. SPIE Vol. 1646, pp. 343-352(1992)